

**A SOUTHERN PLAINS WINTERTIME DUST STORM ASSOCIATED WITH A  
ROBUST UPPER-LEVEL FRONT**

*by*

JONATHAN E. MARTIN

*Department of Atmospheric and Oceanic Sciences  
University of Wisconsin-Madison  
1225 W. Dayton St.  
Madison, WI 53706  
[jemarti1@wisc.edu](mailto:jemarti1@wisc.edu)*

Submitted for publication as a Note in *Monthly Weather Review*  
(July 20, 2007)

## ABSTRACT

Analyses of observations and the output from a numerical simulation are employed to investigate the influence of a robust upper-level front on a significant dust storm that swept across portions of the southern Plains of the United States on 24 February 2007. The dust plume developed well west of the surface cold front associated with a developing surface cyclone and had a notably frontal geometry with its length approximately an order of magnitude greater than its width at maturity.

Air parcel trajectories indicated that air delivered to the top of a deep, dry adiabatic boundary layer over west Texas and southeastern New Mexico originated over southern Utah, in the heart of the cold air beneath a deep upper-level trough that was organizing the broader synoptic flow. The strong subsidence associated with the development of the upper-front supported downward advection of high momentum air (wind speeds  $> 20 \text{ m s}^{-1}$ ) from within the upper-frontal shear zone. The persistent downward momentum advection promoted leakage of high momentum air into the poorly stratified cold dome that was contiguous with the back edge of the upper-frontal zone. Once injected into this region, the  $20 \text{ m s}^{-1}$  air quickly mixed to the surface and produced the dust plume.

A cursory synoptic analysis of several other late winter/early spring dust storms in the middle latitude Northern Hemisphere suggests that upper-level fronts may frequently play a primary role in dust storm production.

## 1. Introduction

On 24 February 2007 a robust upper-level frontal zone migrated across southern New Mexico into central Texas as a vigorous mid-latitude cyclone developed over the Central United States. Coincident with the passage of the upper-level frontal zone aloft over western and central Texas were widespread reports of sustained surface winds of  $20 \text{ m s}^{-1}$  with gusts exceeding  $30 \text{ m s}^{-1}$ . Such high surface winds initiated the development of a significant dust plume that eventually measured roughly 1000 km long and order 100 km wide. This dust plume effected many locations in the Llano Estacado of eastern New Mexico and western Texas and then moved into central Texas hitting Abilene, Dallas, and Wichita Falls, TX as well as Lawton, and Oklahoma City, OK lending the sky an eerie orangy/sepia tone and reducing visibilities below one mile throughout the region. In fact, from 9 AM to 12 noon (LST), visibility dropped to near zero along a stretch of U. S. highway 84 in northwest Garza County, Texas (in the northern Texas panhandle). A band of light snow in the western Texas panhandle dropped between 2 and 3 cm of snow, some of which was brown and mixed with mud drops by virtue of its interaction with the evolving dust plume. Wind gusts exceeding  $28 \text{ m s}^{-1}$  cancelled over 300 departing flights from Dallas-Fort Worth International Airport (DFW) and 90,000 homes and businesses were left without power in the Dallas metropolitan area by 2200 UTC 24 February (Dallas Morning News). The Dallas National Weather Service Forecast Office (NWSFO) reported that the westerly winds associated with this dust event were the strongest in the area in nearly 20 years.

The recurrence of significant dust storms over the southern Great Plains of the United States during the Dust Bowl of the 1930's prompted the first systematic examination of the meteorological conditions attendant with major dust storms. In a pioneering study, Parkinson (1936) identified several conditions routinely associated with such storms. Among these were 1) weakly stable to unstable stratification in the dust source region, and 2) near surface wind speeds in excess of  $15 \text{ m s}^{-1}$  (29 kts), subsequently supported by the analysis of Clements et al. (1963). Parkinson also noted that the majority of dust storms in the southern Great Plains occur in late winter and early spring, a time that coincides with the start of the growing season when both cultivated and uncultivated soils are barren and the polar jet approaches its climatologically lowest latitude of the year. Parkinson also indicted leeside subsidence as a mechanism by which drier, higher momentum air might be introduced into the boundary layer. Deepening and destabilization of the boundary layer in the dust source regions was thought to result from daytime heating which allows mixing of high momentum air downward from aloft, a supposition consistent with the observation of a 1600 LST frequency maximum for dust storms in the region (Pollard 1978).

These ingredients were also identified by Hagen and Woodruff (1973) who considered dust events in the Great Plains as a component of air pollution. Their examination of hourly observations of dusty days during the 1950's at 37 weather stations in the region found southerly winds of  $9 - 13 \text{ m s}^{-1}$  and relative humidities below 70% in 92% of the dusty hours, indicating that the requisite strong winds are also *dry* in dust events. The latter point was also noted by Pollard (1978) who found that as the visibility associated with dust events decreased, the dewpoint depressions increased.

Orgill and Sehmel (1976) investigated the frequency of dust storms in the continental United States and identified the panhandles of Texas and Oklahoma as the location of greatest dust frequency with a bullseye over Lubbock, Texas (see their Fig. 2). The monthly frequency maxima occur in March and April when the strong winds are associated with springtime cyclonic and convective storms. Pollard (1978) indicted surface frontal passages, squall lines, and leeside troughs as the primary synoptic-scale features responsible for generating the strong surface winds that drive dust storms in this region. Orgill and Sehmel also noted that the diurnal frequency maxima is during local afternoon (1200 to 2000 LST) which they attributed to the fact that at such times the boundary layer is at its deepest and turbulent mixing is therefore most pronounced.

A physical link between dust storms and large scale cyclogenesis events was explored by Danielsen (1974). In both of the cases he examined, the encroachment of an upper-level frontal zone on a deep, well mixed, springtime boundary layer over the southern Great Plains initiated the downward mixing of high momentum air to the surface where it forced the lofting of dust and sand. Pauley et al. (1996) found a similar connection in their study of a dust storm in the San Joaquin Valley of California. They implicated the strong downward vertical motion associated with upper-frontal development in transporting high momentum air downward to mid-levels where boundary layer processes then mixed it to the surface, resulting in a dramatic lowering of visibility and a series of collisions involving 164 vehicles on Interstate 5.

The purpose of this note is to document the evolution of the 24 February dust plume, as seen from the GOES-12 satellite, and to describe its physical connection with a robust upper-level front which penetrated deep into the troposphere. The paper is

organized in the following manner. In section 2 the satellite view of the evolving dust plume is presented along with an overview of the synoptic setting in which the evolution took place. In section 3 the structure of the upper-level frontal zone is interrogated with observations and a numerical simulation of the event performed using the Weather Research and Forecasting Model (WRF). Conclusions regarding the physical connection between the upper-front and the dust plume are given in Section 4 where a discussion of the results is also included.

## **2. Synoptic Overview**

### *a. The dust plume*

The dust plume of interest first appeared at 1500 UTC 24 February 2007 near Hobbs, New Mexico in the far southeast corner of that state. Figure 1 shows an hourly sequence of GOES-12 visible images from 1915 UTC to 2215 UTC 24 February. As the plume progressed eastward across northcentral Texas and evolved, it developed a distinctly frontal geometry. Early on in the event (1915 UTC) the dust plume was only slightly longer than it was wide (Fig. 1a). The plume then steadily lengthened to over 1000 km in length while retaining a width of order 100 km by 2215 UTC (Fig. 1d). After 2300 UTC the plume continued to move eastward with dust reported at Fort Smith, AR at 0000 UTC 25 February and as far east as Little Rock, AR by 0400 UTC (not shown). In

fact, dust from this plume was clearly visible in MODIS imagery off the Texas and Louisiana Gulf coasts throughout the day on February 25.<sup>1</sup>

*b. Synoptic setting*

At 1200 UTC 24 February 2007, an elongated sea-level pressure minimum of 988 hPa stretched across southwestern Kansas and the Oklahoma panhandle (Fig. 2a). Trailing southward from this depression was a surface cold front that stretched through central Oklahoma and eastern Texas. A secondary trough of low pressure, associated with a continuous windshift from westerly to northwesterly, draped through northern New Mexico. Northerly winds in excess of  $15 \text{ m s}^{-1}$  were fairly widespread north of this trough in Colorado. A belt of winds between 10 and  $15 \text{ m s}^{-1}$  was found between the surface cold front and the secondary trough along a line from Childress, TX (CDS) to Lubbock, TX (LBB), to Guadalupe Pass, TX (GDP). It was in this latter region of high winds, well west of the surface cold front, that the dust storm developed.

At 850 hPa, the geopotential minimum was located in central Kansas with a sharp cold front trailing to its south (Fig. 2b). The region of strong surface winds from within which the dust storm would develop was located to the west of the 850 hPa cold frontal position. The circulation center at 500 hPa was located over the Texas/Oklahoma/New Mexico border at this time with a wind speed maximum of  $60 \text{ m s}^{-1}$  at El Paso, TX (EPZ) (Fig. 2c). Also noteworthy is the sharp temperature contrast at this level, indicative of the

---

<sup>1</sup> Imagery can be viewed at the following website  
[http://alg.umbc.edu/usaq/archives/2007\\_02.html](http://alg.umbc.edu/usaq/archives/2007_02.html).

presence of a strong upper-level front over southern New Mexico and the western panhandle of Texas.

A vertical cross-section through the upper-front is shown in Fig. 3. The upper-front extends from the tropopause, near Albuquerque, New Mexico (ABQ), to nearly 800 hPa between El Paso, Texas (EPZ) and Guyamas, Mexico (MMGM) at this time. Consequently, the high wind speeds that constitute the zone of horizontal and vertical shear associated with the front extend nearly to the surface between the same two stations. The sounding at EPZ demonstrates a deep, dry adiabatic layer extending from the surface to ~650 hPa where a temperature inversion identifies the base of the upper-frontal zone and another ending at nearly 500 hPa identifies the top of the zone (Fig. 4a). The sounding at Midland, TX (MAF) tells a similar story at this time (Fig. 4b) with a deep dry adiabatic layer extending from the surface to ~760 hPa. Above this layer the winds back slightly to about 650 hPa where a slight inversion signals the weak, lower fringes of the upper-front. Both soundings suggest an environment which, upon being subjected to insolation and daytime heating, is susceptible to rapid turbulent mixing of high momentum air down to the surface. In fact, winds in excess of  $25 \text{ m s}^{-1}$  sat just above 800 hPa over EPZ at this time (Fig. 3).

Meteorograms at three different stations affected by the dust share some similarities. At Hobbs, New Mexico (HOB), a steady rise in temperature occurs throughout the day accompanied by slight drying (Fig. 5a). A windshift from southwesterly to westerly coincides with the peak gusts (of nearly  $25 \text{ m s}^{-1}$ ) which accompanies the first reports of dust associated with this event.

The trace at Wichita Falls, TX (SPS) denotes passage of a surface cold front at 1100 UTC which, though accompanied by a windshift, is not associated with a wind speed change (Fig. 5b). The windspeed increases dramatically between 1500 and 1600 UTC, when the dewpoint reaches its minimum, and gustiness increases. By 1800 UTC gusts up to  $25 \text{ m s}^{-1}$  are associated with blowing dust at SPS as the wind gradually veers to the west.

At Fort Worth, TX (NFW) there is a sharp windshift at 1400 UTC accompanied by a dewpoint drop but no temperature change (Fig. 5c), reminiscent of a drytrough passage as described in Martin et al. (1995). The dewpoint reaches its minimum 5 hours later coincident with peak gustiness, the lofting of dust, and a veering to westerly winds. It is likely that the drying and increased gustiness are the results of downward mixing of drier, higher momentum air from aloft.

Thus, analysis of the observations suggests that a deeply penetrating upper-frontal zone was positioned over southern New Mexico and western Texas at 1200 UTC. We hypothesize that the high momentum air necessary to produce the subsequent dust storm originated in the horizontal and vertical shear zone associated with this front and was advected downward to the top of the planetary boundary layer by the very subsidence responsible for the upper-frontogenesis. Upon delivery to the top of the mixed layer, this air was easily mixed to the surface (further reducing its relative humidity) through turbulence induced by insolation. Consequently, the upper-front and associated upper-frontogenesis were proximate causes of the dust storm. In order to demonstrate these physical connections more conclusively, we employ a fine-scale numerical simulation of this event using the Weather Research and Forecasting (WRF) model. In the next section

we describe the simulation and provide an analysis of the structural and dynamical evolution of the upper-front by means of consideration of several characteristic air parcel trajectories associated with this event.

### **3. Model Simulation and analysis**

#### *a. Model description*

The simulation employed in this study was performed using a recent version of the Weather Research and Forecasting (WRF) modeling system with the Advanced Research WRF (ARW) solver as described by Skamarock et al. (2005). The six-hourly Global Final Analysis (FNL) data set provided by the National Center for Environmental Prediction (NCEP) is utilized for the initial fields and boundary conditions with the boundaries nudged between each analysis time. Specific physical parameterizations include the Ferrier new-Eta microphysics scheme (Ferrier et al. 2002), Dudhia (1989) shortwave radiation and the Rapid Radiative Transfer Model (RRTM, Mlawer et al. 1997) longwave radiation schemes, the KF2 cumulus scheme modified by Kain and Fritsch (1990, 1993), and the Yonsei University (YSU) planetary boundary layer scheme (Hong and Pan, 1996, Hong et al. 2006). The simulation was initialized at 0000 UTC 24 February 2007 and was run for 48 h employing a 91 x 61 grid mesh with 31 vertical levels and a horizontal grid spacing of 54 km over the domain shown in Fig. 6.

#### *b. Model evaluation*

As most of the subsequent analysis will center on the structure, evolution, and progression of the upper-level front and its associated kinematic fields, a limited model evaluation is offered here. The 12 h forecast of the 500 hPa geopotential height and temperature is shown in Fig. 7a. This forecast compares well with the analysis of the observations presented in Fig. 2c though is slightly warmer at the core of coldest air over north central New Mexico. Similar comparisons between 12 h model forecasts of the other vertical levels displayed in Fig. 2 are equally faithful (not shown). A model forecast vertical cross-section, valid at 1200 UTC 24 February and chosen to mimic the observed section shown in Fig. 3, is presented in Fig. 7b. The thermal structure is reproduced rather well as is the region of wind speeds greater than  $20 \text{ m s}^{-1}$  that lies beneath the upper-level frontal zone. A significant difference is that the jet core is significantly slower in the model section than in the observations.<sup>2</sup> Accounting for this discrepancy is beyond the scope of the present study. However, a discussion of its possible dynamical implications is warranted.

Based upon consideration of the geostrophic forcing term in the Sawyer (1956)-Eliassen (1962) frontal circulation equation, Shapiro (1981) hypothesized that cold air advection in the presence of cyclonic shear would shift the thermally direct (indirect) ageostrophic circulation associated with the confluent (diffluent) jet entrance (exit) region toward the warm (cold) side of the frontal zone, thus providing a circumstance in which the subsidence maxima would be located beneath the jet core. This hypothesis was later

---

<sup>2</sup> El Paso, TX (EPZ) reported a  $70 \text{ m s}^{-1}$  jet at 482 hPa (Fig. 4a) before its wind speed and direction were lost. Even the Rapid Update Cycle (RUC) analysis at 1200 UTC 24 February grossly underestimates the speed of the jet core.

confirmed in a primitive equation modeling study by Keyser and Pecnick (1985). Since the observations portray a flow that was, indeed, characterized by cold air advection in cyclonic shear (Fig. 2c), a slower jet in the forecast would likely mean smaller downward vertical motions beneath the jet core in the forecast than in the observations. Thus, the downward vertical motions near the jet core shown in Fig. 7b, though of substantial magnitude, are likely an underestimate of reality. Even so, downward vertical motion exceeding  $10 \text{ cm s}^{-1}$ , associated with the vigorous upper-level frontogenesis occurring at 1200 UTC, touches the ground over central New Mexico in this forecast. A  $10 \text{ cm s}^{-1}$  downdraft implies downward vertical displacements of 1080 m in three hours. Recall that the 1200 UTC sounding at EPZ (El Paso, Texas) reported wind speeds in excess of  $25 \text{ m s}^{-1}$  at 780 hPa (only 882 m above the surface at EPZ). Thus, the subsidence associated with the developing upper-front and ongoing frontogenesis was, by itself, sufficient to drag the high momentum air down to the surface and initiate the lofting of dust. Despite the likely underestimate of the downward vertical motion associated with the upper-frontogenesis in the model simulation, we confidently employ the model output to trace the connection between the high momentum, lower tropospheric air responsible for the dust storm and the structure and evolution of the upper-level front.

### *c. Trajectory analysis*

Recall that the 1200 UTC soundings at Midland (MAF) and El Paso (EPZ), Texas showed a deep, well mixed boundary layer extending from the surface to between 750 hPa (MAF) and 700 hPa (EPZ) (Fig. 4). Given the rather rapid vertical mixing that can

occur in such a well mixed layer, parcels of air that arrived at the top of the observed boundary layer (2.9 km) at 1500 UTC over southeast New Mexico were considered a likely source of the high momentum surface air responsible for producing the dust plume. In this section the origin of such air parcels is considered through analysis of back trajectories initialized there. The path of one such representative trajectory is shown in Fig. 8. At 0500 UTC 24 February the parcel was located over southern Utah, at 5.11 km, near the center of the 500 hPa cold dome to the northeast of the developing upper-frontal baroclinic zone (Fig. 9a). A model forecast vertical cross-section (along line C-C' in Fig. 9a) at this time illustrates the developing nature of this upper-frontal zone as a  $10 \text{ cm s}^{-1}$  downdraft is located directly beneath the jet core (Fig. 10a). The air parcel is located in the cold dome directly beneath and to the north of the upper-frontal zone. This cold dome represents the most poorly stratified column in the entire domain with a lapse rate barely smaller than the dry adiabatic rate. It is noteworthy that such poorly stratified air is contiguous with the sloping baroclinic zone that constitutes the upper-frontal zone as well as the upper-frontal shear zone delineated by the  $20 - 50 \text{ m s}^{-1}$  isotachs. At this time it is clear that  $20 \text{ m s}^{-1}$  winds are completely contained within this upper-frontal shear zone. In fact, the  $20 \text{ m s}^{-1}$  isotach forms the kinematic backbone of the upper-frontal zone at this time as well as at earlier times (not shown).

Two hours later the 500 hPa temperature contrast remained very strong and was located to the southwest of the parcel location which remained in the heart of the cold air at this level (Fig. 9b). Continued subsidence beneath the jet core at this time (Fig. 10b) testifies to the continued intensification of the upper-front. Note the  $20 \text{ m s}^{-1}$  isotach continued to anchor the back edge of the upper-frontal zone at 0700 UTC and the poorly

stratified cold dome remained contiguous with this back edge. It is also clear from Figs 10a and 10b that the substantial downward vertical motion characterizing this developing upper-front was also promoting downward advection of the high momentum air that constituted the upper-frontal shear zone. Consider, for instance, the Xs in Fig. 10a and 10 b. In Fig. 10a, the X represents the location of the intersection of the  $20 \text{ m s}^{-1}$  isotach with the 294 K isentrope, located at  $\sim 580 \text{ hPa}$  at 0500 UTC. By 0700 UTC, the  $20 \text{ m s}^{-1}$  isotach had pushed through the 294 K isentrope to  $\sim 620 \text{ hPa}$  – likely a result of the downward vertical motion of about  $7 \text{ cm s}^{-1}$  which, acting for two hours, implies a descent of  $\sim 500 \text{ m}$ .

By 0900 UTC, the parcel was still located in the center of the cold air at 500 hPa but was now closer to the cold edge of the upper-frontal baroclinic zone at that level (Fig. 9c). Two important differences in the vertical cross-section normal to the front at this time stand out (Fig. 10c). First, the cold dome stratification had increased as nocturnal cooling of the surface continued. Most importantly, however, the  $20 \text{ m s}^{-1}$  isotach had been deformed and no longer smoothly defined the back edge of the upper-frontal shear zone. In fact, the representative air parcel is contained within the  $20 \text{ m s}^{-1}$  isotach. Though the subsidence beneath the jet core was weaker at this time than at the prior two times, it appears as though the combination of persistent downward advection of high momentum air by the upper-frontogenetic subsidence coupled with the proximity of a poorly stratified cold dome beneath and to the northeast of the upper-frontal zone had led to a “leakage” of frontal shear zone momentum into the poorly stratified cold dome.

Two hours later, the 500 hPa thermal contrast had intensified slightly and the representative parcel, though still located in the cold air on the poleward side of the 500

hPa baroclinic zone, was closer to the cold edge of that zone than it had been previously (Fig. 9d). The vertical cross-section through the front at this time illustrates intensified subsidence beneath the jet core, continued upper-frontogenesis, and continued downward advection of frontal shear zone momentum. The  $20 \text{ m s}^{-1}$  isotach now covered a substantial portion of the surface over western and central New Mexico just a few hours before the first reported dust in this southeastern portion of that state. The isotachs in Fig. 10d reinforce the impression of a “leak” of high momentum air from the back edge of the frontal shear zone.<sup>3</sup>

By 1300 UTC the representative parcel was located on the cold edge of the 500 hPa baroclinic zone which was considerably more intense than it had been just a few hours before (Fig. 9e). The vertical motion pattern along the cross-section at this time featured a strong downdraft that cut through the jet core (Fig. 10e). Strong subsidence reached the surface over southeast New Mexico at the center of the region of surface winds in excess of  $20 \text{ m s}^{-1}$ . At this time, even the  $30 \text{ m s}^{-1}$  isotach from the frontal shear zone was impinging on the poorly stratified air of the cold dome. The parcel of interest was embedded in the core downdraft at this time and had already subsided nearly 1.6 km in the previous 8 hours. The “leakage” of high momentum air from the upper-frontal shear zone appeared to be strongest at this time.

Finally, by 1500 UTC, the parcel was located at the top of the mixed layer (2.9 km) in far southeastern New Mexico, beneath the center of the 500 hPa baroclinic zone (Fig. 9f). The vertical cross-section at this time again portrays an intensifying upper-frontal zone with subsidence maximized beneath the jet core (Fig. 10f). The persistent

---

<sup>3</sup> It is interesting to note that the  $20 \text{ m s}^{-1}$  isotach in Fig. 3 has a similar geometry to that portrayed in Fig. 10d.

subsidence had, by this time, deformed the  $30 \text{ m s}^{-1}$  isotach in a manner similar to the deformation of the  $20 \text{ m s}^{-1}$  isotach at 0900 UTC (Fig. 10c), such that  $30 \text{ m s}^{-1}$  air from the upper-frontal shear zone was hovering slightly above the surface just poleward of the upper-front. The representative parcel had by now clearly acquired a wind speed in excess of  $30 \text{ m s}^{-1}$  which the foregoing analysis suggests originated in the high momentum shear zone of the developing upper-front.

As daytime heating progressed, the boundary layer deepened over central Texas allowing different air parcels, with similar physical connection to the upper-front and similar histories along their trajectories, to be delivered to the top of the midday mixed layer in central Texas (not shown). Such parcels were likely mixed to the surface in the dry adiabatic boundary layer and contributed to the maintenance of the dust storm in this case.

#### **4. Summary and Conclusions**

On 24 February 2007 a significant dust storm swept across eastern New Mexico, central Texas and parts of Oklahoma. The dust plume that developed in this event had a notably frontal geometry with its length approximately an order of magnitude greater than its width at maturity. The dust plume developed well west of a surface cold front associated with a developing surface cyclone located in southwestern Kansas and Oklahoma and was associated with gusty west winds and a persistent drying of the lower troposphere, characteristics consistent with systematic downward mixing of air from the top of the boundary layer. The dust plume and its evolution were spatially correlated

with the passage of an intensifying upper-level frontal zone which was also a component of the concurrent surface cyclogenesis.

Analysis of both conventional observations and the output from a numerical simulation of the event performed using the WRF model were used to interrogate this case. A deep dry adiabatic layer existed over west Texas and southeast New Mexico at 1200 UTC 24 February – three hours before the dust plume first developed. Air parcel trajectories indicated that air that was delivered to the top of this mixed layer at 1500 UTC originated over southern Utah, in the heart of the cold air beneath a deep upper level trough which was organizing the broader synoptic flow. The weakly stratified cold dome air was, as is characteristic of such settings, contiguous with the back edge of the upper-frontal zone. The upper baroclinic zone was characterized by cold air advection in cyclonic shear and so possessed a potent subsidence maxima beneath the jet core that promoted upper-frontogenesis via tilting. This same subsidence supported downward advection of high momentum air from within the upper-frontal shear zone. Given the poor stratification of the adjacent cold dome, the persistent downward advection promoted leakage of high momentum air from the frontal shear zone into the poorly stratified cold dome. Once injected into this region, the  $20 \text{ m s}^{-1}$  air quickly mixed to the surface and, eventually, produced the dust plume. As daytime heating deepened the boundary layer in central Texas, the strong winds were continually mixed to the surface and acted to maintain the dust plume. The frontal scale geometry of the plume as well as its location directly beneath the 500 hPa baroclinic zone are both consistent with the notion that the developing upper-front played a primary role in the production and maintenance of the dust plume.

The fact that upper-level fronts can play important roles in a variety of surface sensible weather events invests them with continued research and operational relevance. Most recently, upper-fronts have been implicated as major players in shaping some wildfire environments (e.g. Zimet et al. 2007) and have been suggested as agents in the production of high wind events in the mountainous terrain of the western United States (C. Smallcomb, NWS-Reno, personal communication). To our knowledge, the only prior study that implicates upper-frontal processes in initiating a dust storm over the Central Plains of the United States is that of Danielsen (1974) who found that the encroachment of an upper-level front on a deep, well mixed, springtime boundary layer initiated the downward mixing of high momentum air to the surface where it forced the lofting of dust and sand. In their more detailed study of a dust storm in the San Joaquin Valley of California, Pauley et al. (1996) suggested a similar connection. Though neither of these studies examined air parcel trajectories in their analyses, and therefore offer somewhat circumstantial evidence of a physical connection between upper-frontal processes and the dust storms, these are the only published studies suggesting that upper-fronts are involved in the production of dust storms.

The southern plains of the United States is not the only location in the Northern Hemisphere prone to late winter/early spring dust storms. In fact, in their climatology of Mongolian dust storms, Natsagdorj et al. (2003) found that over 60% of dust storms in Mongolia occur in the spring. They also noted an afternoon frequency maximum, a veering to northwesterly winds and a lowering of relative humidity in Mongolian dust events; all characteristics found in the present case. They refer specifically to a severe dust event that occurred from 27-30 November 1991 but do not examine the synoptic

conditions attendant with that even in any detail. A detailed synoptic overview of the severe Mongolian dust storm of 6-7 April 2001 is presented by Liu et al. (2004). Particularly noteworthy in this event was the fact that the lofted dust crossed the Pacific Ocean and eventually arrived in North America. cursory examination of the National Centers for Environmental Prediction (NCEP) Reanalysis data<sup>4</sup> for that case suggests a connection between the dust storm and the progression of a vigorous upper-front over southern Mongolia. A similar such connection appears to exist for two other Mongolian cases discussed by Shao et al. (2003) as well as for some late winter/early spring dust storms in North Africa (e.g. Knippertz and Fink 2006), the southeastern Mediterranean (e.g. Alpert and Ganor 1993), 2/3 of the cases of heavy dust events in the southcentral United States examined in Gillette et al. (1978) (see their Table 4), as well as several winter/early spring dust storms in the vicinity of the Arabian Peninsula (Barhan et al. 2004). The relatively high percentage of dust storm cases that appear to have a physical connection to developing upper-level fronts adds another important, high impact weather event to the list of those associated with upper-frontal processes and clearly identifies further study of the precise physical mechanisms and synoptic features involved in producing these storms as a worthy research priority.

ACKNOWLEDGEMENTS: The author would like to thank Mr. Andrew Hulme for running the WRF model run used in this analysis. This work was partially funded by the a grant from the National Science Foundation, ATM-0452318.

---

<sup>4</sup> We used NCEP Reanalysis Plotter developed and maintained by Dr. Christopher Godfrey at <http://weather.ou.edu/~cgodfrey/reanalysis/>.



## REFERENCES

- Alpert, P., and E. Ganor, 1993: A jet stream associated heavy dust storm in the western Mediterranean. *J. Geophys. Res.*, **98**, 7339-7349.
- Barhan, J., H. Kutiel, and P. Alpert, 2004: Climatology of dust storms in North Africa and the Arabian Peninsula based on TOMS data. *Indoor Built Env.*, **13**, 407-419.
- Clements, T., J. F. Mann, R. O. Stone, and J. L. Eymann, 1963: A study of windborne sand and dust in desert areas. Technical Report ES-8, Earth Sciences Div., I/S, Army National Laboratories.
- Danielsen, E. F., 1974: The relationship between severe weather, major dust storms and rapid large-scale cyclogenesis (II). *Subsynoptic Extratropical Weather Systems: Observations, Analysis, Modeling and Prediction*, Vol. 2, M. Shapiro, Ed., National Center for Atmospheric Research, 226-241.
- Dudhia, J., 1989: Numerical study of convection observed during the winter monsoon experiment using a mesoscale two-dimensional model. *J. Atmos. Sci.*, **46**, 3077-3107.
- Eliassen, A., 1962: On the vertical circulation in frontal zones. *Geophys. Publ.*, **24**(4), 147-160.

Ferrier, B. S., Y. Jin, Y. Lin, T. Black, E. Rogers, and G. DiMego, 2002: Implementation of a new grid-scale cloud and precipitation scheme in the NCEP Et model. *15<sup>th</sup> Conference on Numerical Weather Prediction*, Amer. Meteor. Soc., San Antonio, TX, 280-283.

Gillette, D. A., Clayton, R. N., Mayeda, T. K., Jackson, M. L., and Sridhar, K., 1978: Tropospheric aerosols from some major dust storms of the Southwestern United States. *J. Appl. Met.*, **17**, 832-845.

Hagen, L. J., and N. P. Woodruff, 1973: Air pollution from duststorms in the Great Plains. *Atmospheric Environment*, **7**, 323-332.

Hong, S.-Y., and H.-L. Pan, 1996: Nonlocal boundary layer vertical diffusion in a medium-range forecast model. *Mon. Wea. Rev.*, **124**, 2322-2339.

\_\_\_\_\_, Y. Noh, and J. Dudhia, 2006: A new vertical diffusion package with an explicit treatment of entrainment processes. *Mon. Wea. Rev.*, **134**, 2318-2341.

Kain, J. S. and J. M. Fritsch, 1990: A one-dimensional entraining/detraining plume model and its application in convective parameterization. *J. Atmos. Sci.*, **47**, 2784-2802.

\_\_\_\_\_, and \_\_\_\_\_, 1993: Convective parameterization for mesoscale models:

- The Kain-Fritsch scheme. *The Representation of Cumulus Convection in Numerical Models, Meteor. Monogr.*, No. 46, Amer. Meteor. Soc., 165-170.
- Keyser, D., and M. J. Pecnick, 1985: A two-dimensional primitive equation model of frontogenesis forced by confluence and horizontal shear. *J. Atmos. Sci.*, **42**, 1259-1282.
- Knippertz, P. and A. Fink, 2006: Synoptic and dynamic aspects of an extreme springtime Saharan dust outbreak. *Quart. J. Roy. Met. Soc.*, **132**, 1153-1177.
- Liu, J.-T., X.-G. Jiang, X.-J. Zheng, L. Kang, and F.-Y., Qi, 2004: An intensive Mongolian cyclone genesis induced severe dust storm. *Terr., Atm., and Oceanic Sciences*, **15**(5), 1019-1033.
- Martin, J. E., J. D. Locatelli, P. V. Hobbs, P.-Y. Wang, and J. A. Castle, 1995: Structure and evolution of winter cyclones in the Central United States and their effects on the distribution of precipitation. Part I: A synoptic-scale rainband associated with a dryline and a lee trough. *Mon. Wea. Rev.*, **123**, 241-264.
- Mlawer, E. J., S. J. Taubman, P. D. Brown, and M. J. Iacono, 1997: Radiative transfer for inhomogeneous atmospheres: RRTM, a validated correlated-k model for the longwave. *J. Geophys. Res.*, **102**, 16 663 – 16 682.

- Natsagdorj, L., D. Jugder, and Y. S. Chung, 2003: Analysis of dust storms observed in Mongolia during 1937-1999. *Atmospheric Environment*, **37**, 1401-1411.
- Orgill, M. M., and G. A. Sehmel, 1976: Frequency and diurnal variation of dust storms in the contiguous U. S. A.. *Atmospheric Environment*, **10**, 813-825.
- Parkinson, G. R., 1936: Dust storms over the Great Plains: Their causes and forecasting. *Bull. Amer. Meteor. Soc.*, **17**, 127-135.
- Pauley, P. M., N. L. Baker, and E. H. Barker, 1996: An observational study of the “Interstate 5” dust storm case. *Bull. Amer. Meteor. Soc.*, **77**, 693-720.
- Pollard, M. C., 1978: Guidelines for forecasting dust storms in the southern Great Plains. *Natl. Wea. Dig.*, **3**(4), 40-44.
- Sawyer, J. S., 1956: The vertical circulation at meteorological fronts and its relation to frontogenesis. *Proc. Roy. Soc. London*, **A234**, 346-362.
- Shao, Y., Y. Yang, J. Wang, Z. Song, L. Leslie, C. Dong, Z. Zhang, Z. Lin, Y. Kanai, S. Yabuki, and Y. Chin, 2003: Northeast Asian dust storms: Real-time numerical prediction and validation. *J. Geophys. Res.*, **108**(D22), 4691, doi:10.1029/2003JD003667.

Shapiro, M. A., 1981: Frontogenesis and geostrophically forced secondary circulations in the vicinity of jet stream-frontal zone systems. *J. Atmos. Sci.*, **38**, 954-973.

Skamarock, W. C., J. B. Klemp, J. Dudhia, D. O. Gill, D. M. Barker, W. Wang, and J. G. Powers, 2005: A description of the advanced research WRF version 2. NCAR Tech Note NCAR/TN-468+STR, 88 pp. {Available from UCAR Communications, P. O. Box 3000, Boulder, CO 80307}.

Zimet, T. K., J. E. Martin, and B. E. Potter, 2007: The influence of an upper-level frontal zone on the Mack Lake wildfire environment. *Met. Applications*, **14**, 131-147.

## FIGURE CAPTIONS

Fig. 1. GOES-12 visible satellite images at (a) 1915 UTC, (b) 2015 UTC, (c) 2115 UTC, and (d) 2215 UTC 24 February 2007. Dust plume is indicated by the arrow in each panel.

Fig. 2. (a) Sea-level pressure analysis at 1200 UTC 24 February 2007. Solid lines are isobars (hPa) labeled and contoured every 4 hPa. Conventional frontal symbols indicate positions of surface fronts with dashed cold frontal symbol indicating secondary surface cold front. For each surface station the following data are shown: temperature ( $^{\circ}\text{C}$ , to the upper left of the station symbol), dewpoint ( $^{\circ}\text{C}$ , to the lower left of the station symbol), sea-level pressure (labeled in hPa, to the upper right of the station symbol), wind direction and speed, skycover and present weather. Sky cover is shown using the following symbols: open circle – clear, one-quarter shaded circle – scattered clouds, one-half shaded circle – broken clouds, three-quarters shaded circle – mostly cloudy, fully shaded circle – overcast. Wind speeds are indicated by half barb -  $< 2.5 \text{ m s}^{-1}$ , short barb –  $2.5 \text{ m s}^{-1}$ , long barb –  $5 \text{ m s}^{-1}$ , flag –  $25 \text{ m s}^{-1}$ . Stations in shaded circles are specifically mentioned in the text. (b) 850 hPa geopotential height (solid lines) and temperature (dashed lines) at 1200 UTC 24 February 2007. Geopotential height labeled in dam and contoured every 3 dam. Temperature labeled in  $^{\circ}\text{C}$  and contoured every  $2^{\circ}\text{C}$ . For each station the following data are shown: temperature ( $^{\circ}\text{C}$ , to the upper left of the station symbol), dewpoint depression ( $^{\circ}\text{C}$ , to the lower left of the station symbol), geopotential height (m, with the thousands digit missing, to the upper right of the station symbol).

Wind speed and direction indicated as in Fig. 2a. (c) 500 hPa temperature and geopotential height at 1200 UTC 24 February 2007. Analyzed as in Fig. 2b except geopotential height contoured every 6 dam. Vertical cross section along line A-A' is shown in Fig. 3.

Fig. 3. Vertical cross section, along line A-A' in Fig. 2c, from Denver, Colorado (DNR), to Albuquerque, New Mexico (ABQ), to El Paso, Texas (EPZ), to Guyamas, Mexico (MMGM) at 1200 UTC 24 February 2007. Thick solid lines are isentropes contoured every 3 K. Thin dashed lines are isotachs normal to the cross section, labeled in  $\text{m s}^{-1}$  and contoured every  $10 \text{ m s}^{-1}$  beginning at  $0 \text{ m s}^{-1}$ . The bold dashed line is the  $25 \text{ m s}^{-1}$  isotach.

Fig. 4. (a) Vertical sounding (Stüve diagram) at El Paso, Texas (EPZ) at 1200 UTC 24 February 2007. Thick solid (dashed) line is the temperature (dewpoint). Thin solid (dashed) lines are dry adiabats (isotherms) with values as labeled in K. Wind speed and direction indicated as in Fig. 2a. (b) As for Fig. 4a but for the sounding at Midland, Texas (MAF) at 1200 UTC 24 February 2007.

Fig. 5. (a) Meteorogram from Hobbs, New Mexico (HOB) from 1300 to 2200 UTC 24 February 2007. Top panel includes traces of temperature (solid line, scale on the side), dewpoint (dashed line, scale on the side), and sensible weather. Conventional symbol for dust is shown. Bottom panel shows wind direction (arrows), average wind speed (solid line with scale on sides), and peak gusts (black dots, with scale on sides). (b)

Meteorogram for Wichita Falls, Texas (SPS) from 0800 – 2200 UTC 24 February 2007.

Top and bottom panel as for Fig. 5a. (c) Meteorogram for Fort Worth, Texas (NFW)

from 1200 – 2200 UTC 24 February 2007. Top and bottom panel as for Fig. 5a.

Fig. 6. Gray shaded area represents the domain for the WRF model run used in this study.

Fig. 7. (a) 12 h forecast of 500 hPa geopotential height (solid lines) and temperature (dashed lines) from the WRF model simulation valid at 1200 UTC 24 February 2007.

Geopotential height and temperature labeled and contoured as in Fig. 2c. Vertical cross section along line B-B' is shown in Fig. 7b. (b) 12 h forecast vertical cross section along line B-B' in Fig. 7a from the WRF model simulation valid at 1200 UTC 24 February 2007. Solid lines are isentropes labeled and contoured as in Fig. 3. Dashed lines are isotachs normal to the cross section line labeled and contoured as in Fig. 3. Shading represents model forecast downward vertical motions at increments of  $5 \text{ cm s}^{-1}$  starting at  $-5 \text{ cm s}^{-1}$  decreasing to  $-20 \text{ cm s}^{-1}$ .

Fig. 8. Path of a representative trajectory, described in the text, from 0100 – 1500 UTC 24 February 2007. Thin line with arrow heads on it, in the middle of the shaded shaft, represents the geographic path of the trajectory. The width of the trajectory indicates the height of the air parcel at each two-hour time increment. Bold numbers to the left of the trajectory path indicate the UTC time at which the parcel is located at the intersection of

the bold black lines and the trajectory path line. Italicized numbers to the right of the trajectory path indicate the elevation of the air parcel at each indicated time.

Fig. 9. (a) 5 h forecast of 500 hPa temperature from the WRF model valid at 0500 UTC 24 February 2007. Solid lines are isotherms labeled and contoured as in Fig. 2c. The parcel whose trajectory path is shown in Fig. 8 is located at the black dot at this time. A vertical cross section along line C-C' is shown in Fig. 10a. (b) As for Fig. 9a but a 7 h forecast of 500 hPa temperature valid at 0700 UTC. The parcel whose trajectory path is shown in Fig. 8 is located at the black dot at this time. A vertical cross section along line D-D' is shown in Fig. 10b. (c) As for Fig. 9a but a 9 h forecast of 500 hPa temperature valid at 0900 UTC. The parcel whose trajectory path is shown in Fig. 8 is located at the black dot at this time. A vertical cross section along line E-E' is shown in Fig. 10c. (d) As for Fig. 9a but an 11 h forecast of 500 hPa temperature valid at 1100 UTC. The parcel whose trajectory path is shown in Fig. 8 is located at the black dot at this time. A vertical cross section along line F-F' is shown in Fig. 10d. (e) As for Fig. 9a but a 13 h forecast of 500 hPa temperature valid at 1300 UTC. The parcel whose trajectory path is shown in Fig. 8 is located at the black dot at this time. A vertical cross section along line G-G' is shown in Fig. 10e. (f) As for Fig. 9a but a 15 h forecast of 500 hPa temperature valid at 1500 UTC. The parcel whose trajectory path is shown in Fig. 8 is located at the black dot at this time. A vertical cross section along line H-H' is shown in Fig. 10f.

Fig. 10. (a) 5 h forecast vertical cross section of potential temperature (solid lines), isotachs normal to the cross section (dashed lines) and downward vertical velocity

(shading) valid at 0500 UTC 24 February 2007 along line C-C' in Fig. 9a. Isentropes are labeled in K and contoured every 3 K. Isotachs are labeled in  $\text{m s}^{-1}$  and contoured every  $10 \text{ m s}^{-1}$  starting at  $10 \text{ m s}^{-1}$ . Downward vertical motion labeled in  $\text{cm s}^{-1}$  and shaded as in Fig. 7b. Black dot indicates the position of the representative air parcel at 0500 UTC.

(b) As for Fig. 10a but for a 7 h forecast, along line D-D' in Fig. 9b, valid at 0700 UTC 24 February 2007. (c) As for Fig. 10a but for a 9 h forecast, along line E-E' in Fig. 9c, valid at 0900 UTC 24 February 2007. (d) As for Fig. 10a but for an 11 h forecast, along line F-F' in Fig. 9d, valid at 1100 UTC 24 February 2007. (e) As for Fig. 10a but for a 13 h forecast, along line G-G' in Fig. 9e, valid at 1300 UTC 24 February 2007. (f) As for Fig. 10a but for a 15 h forecast, along line H-H' in Fig. 9f, valid at 1500 UTC 24 February 2007.

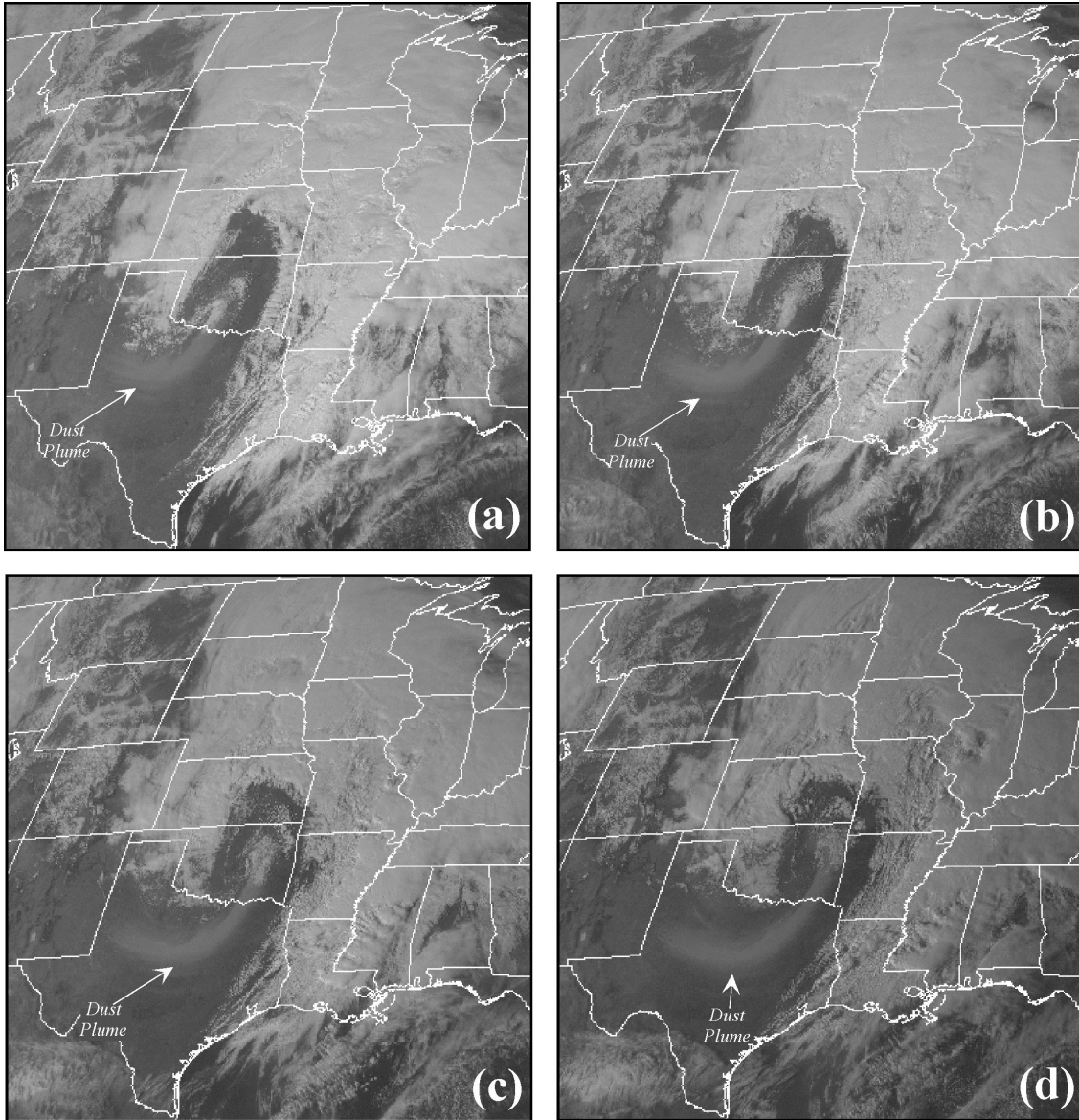


Fig. 1 GOES-12 Visible satellite images at (a) 1915 UTC, (b) 2015 UTC, (c) 2115 UTC, (d) 2215 UTC 24 February 2007. Dust plume is indicated by the arrow in each panel

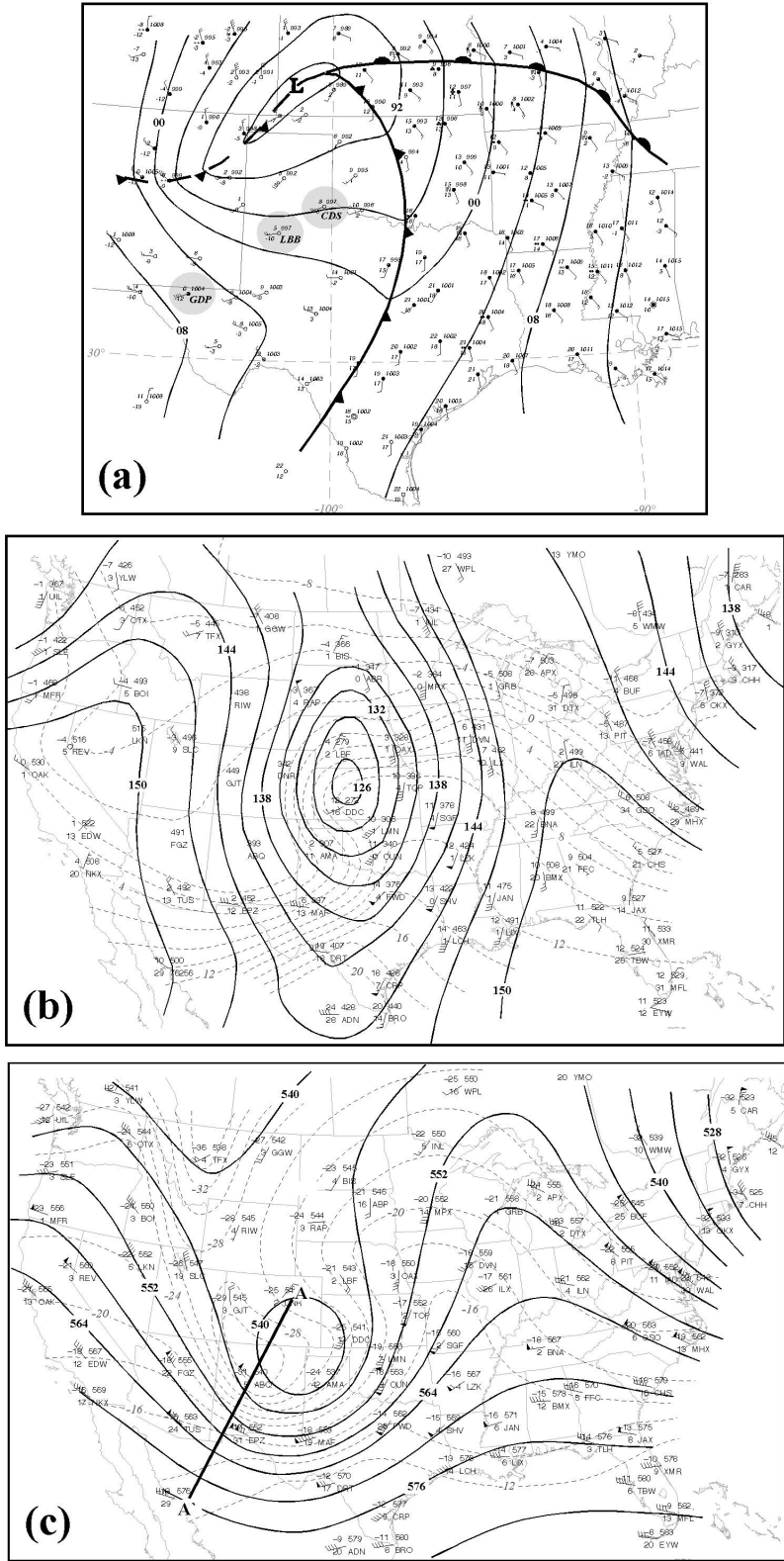


Fig. 2. (a) Sea-level pressure analysis at 1200 UTC 24 February 2007. Solid lines are isobars (hPa) labeled and contoured every 4 hPa. Conventional frontal symbols indicate positions of surface fronts with dashed cold frontal symbols indicating secondary surface cold front. For each surface station the following data are shown: temperature ( $^{\circ}\text{C}$ , to the upper left of the station symbol), dewpoint ( $^{\circ}\text{C}$ , to the lower left of the station symbol), sea-level pressure (labeled in hPa, to the upper right of the station symbol), wind direction and speed, skycover and present weather. Sky cover is shown using the following symbols: open circle – clear, one-quarter shaded circle – scattered clouds, one-half shaded circle – broken clouds, three-quarters shaded circle – mostly cloudy, fully shaded circle – overcast. Wind speeds are indicated by half barb  $< 2.5 \text{ m s}^{-1}$ , short barb  $- 2.5 \text{ m s}^{-1}$ , long barb  $- 5 \text{ m s}^{-1}$ , flag  $- 25 \text{ m s}^{-1}$ . Stations in shaded circles are specifically mentioned in the text. (b) 850 hPa geopotential height (solid lines) and temperature (dashed lines) at 1200 UTC 24 February 2007. Geopotential height labeled in dam and contoured every 3 dam. Temperature labeled in  $^{\circ}\text{C}$  and contoured every  $2^{\circ}\text{C}$ . For each station the following data are shown: temperature ( $^{\circ}\text{C}$ , to the upper left of the station symbol), dewpoint depression ( $^{\circ}\text{C}$ , to the lower left of the station symbol), geopotential height (m, with the thousands digit missing, to the upper right of the station symbol). Wind speed and direction indicated as in Fig. 2a. (c) 500 hPa temperature and geopotential height at 1200 UTC 24 February 2007. Analyzed as in Fig. 2b except geopotential height contoured every 6 dam. Vertical cross section along line A-A is shown in Fig. 3.

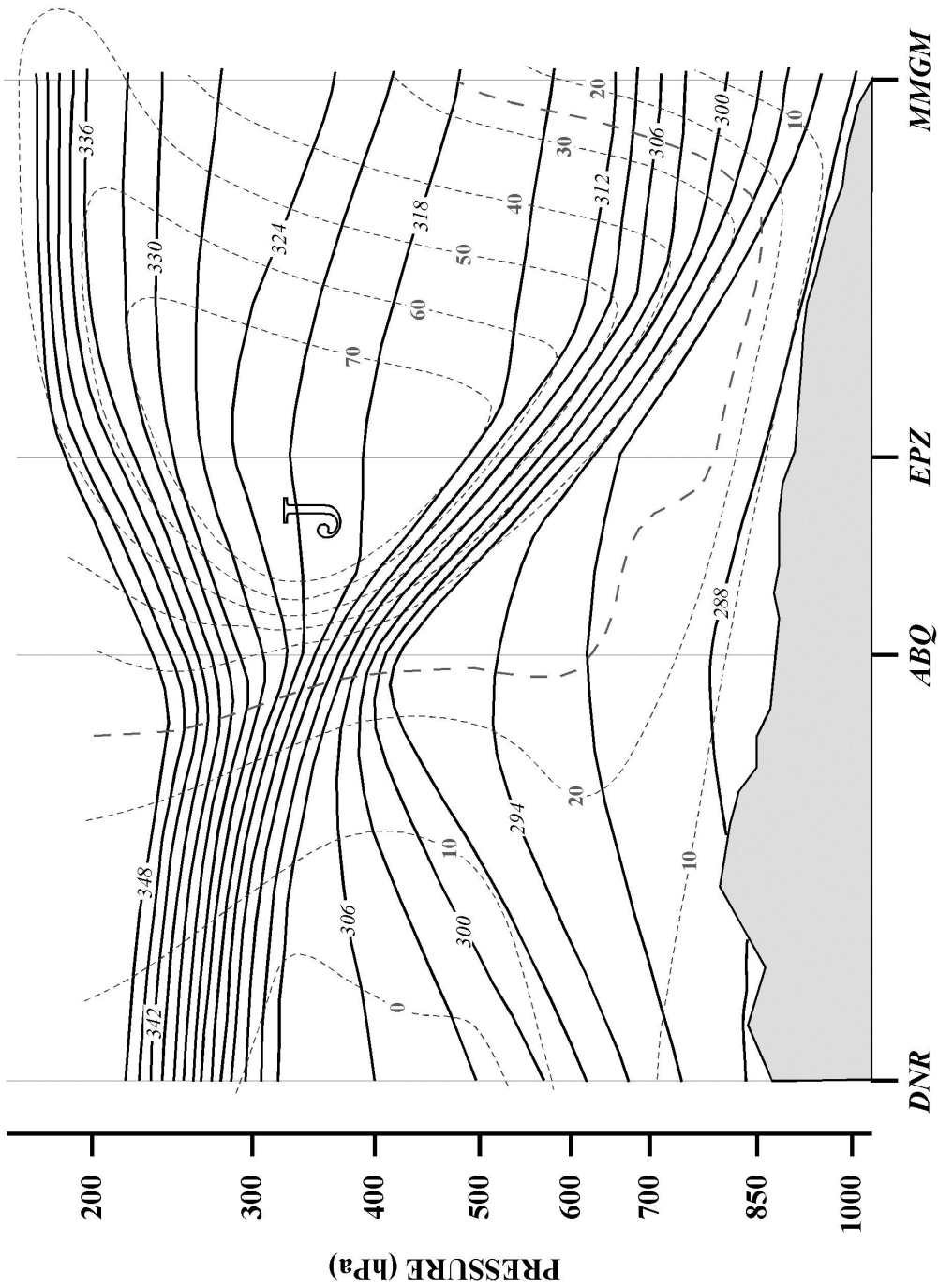


Fig. 3. Vertical cross section, along line A-A' in Fig. 2c, from Denver, Colorado (DNR), to Albuquerque, New Mexico (ABQ), to El Paso, Texas (EPZ), to Guaymas, Mexico (MMGM) at 1200 UTC 24 February 2007. Thick solid lines are isentropes contoured every 3 K. Thin dashed lines are isotachs normal to the cross section, labeled in  $\text{m s}^{-1}$  and contoured every  $10 \text{ m}^{-1}$  beginning at  $0 \text{ m s}^{-1}$ . The bold dashed line is the  $25 \text{ m s}^{-1}$  isotach.

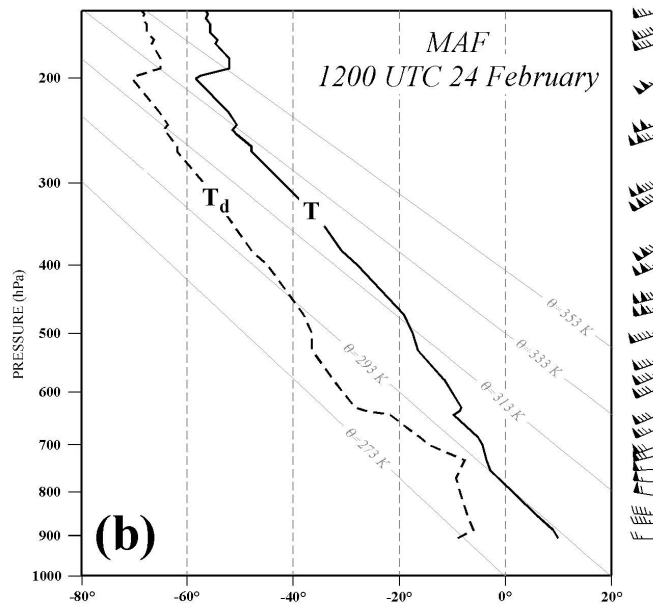
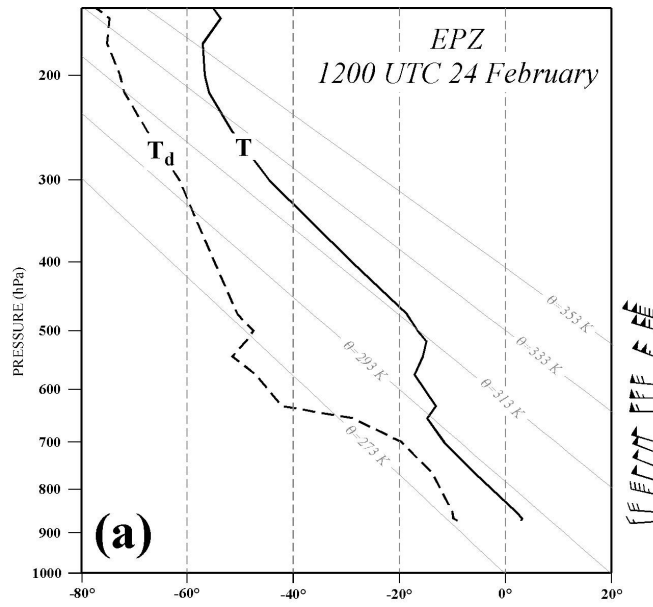


Fig. 4. (a) Vertical sounding (Stüve diagram) at El Paso, Texas (EPZ) at 1200 UTC 24 February 2007. Thick solid (dashed) line is the temperature (dewpoint). Thin solid (dashed) lines are dry adiabats (isotherms) with values as labeled in K. Wind speed and direction indicated as in Fig. 2a. (b) As for Fig. 4a but for the sounding at Midland, Texas (MAF) at 1200 UTC 24 February 2007.

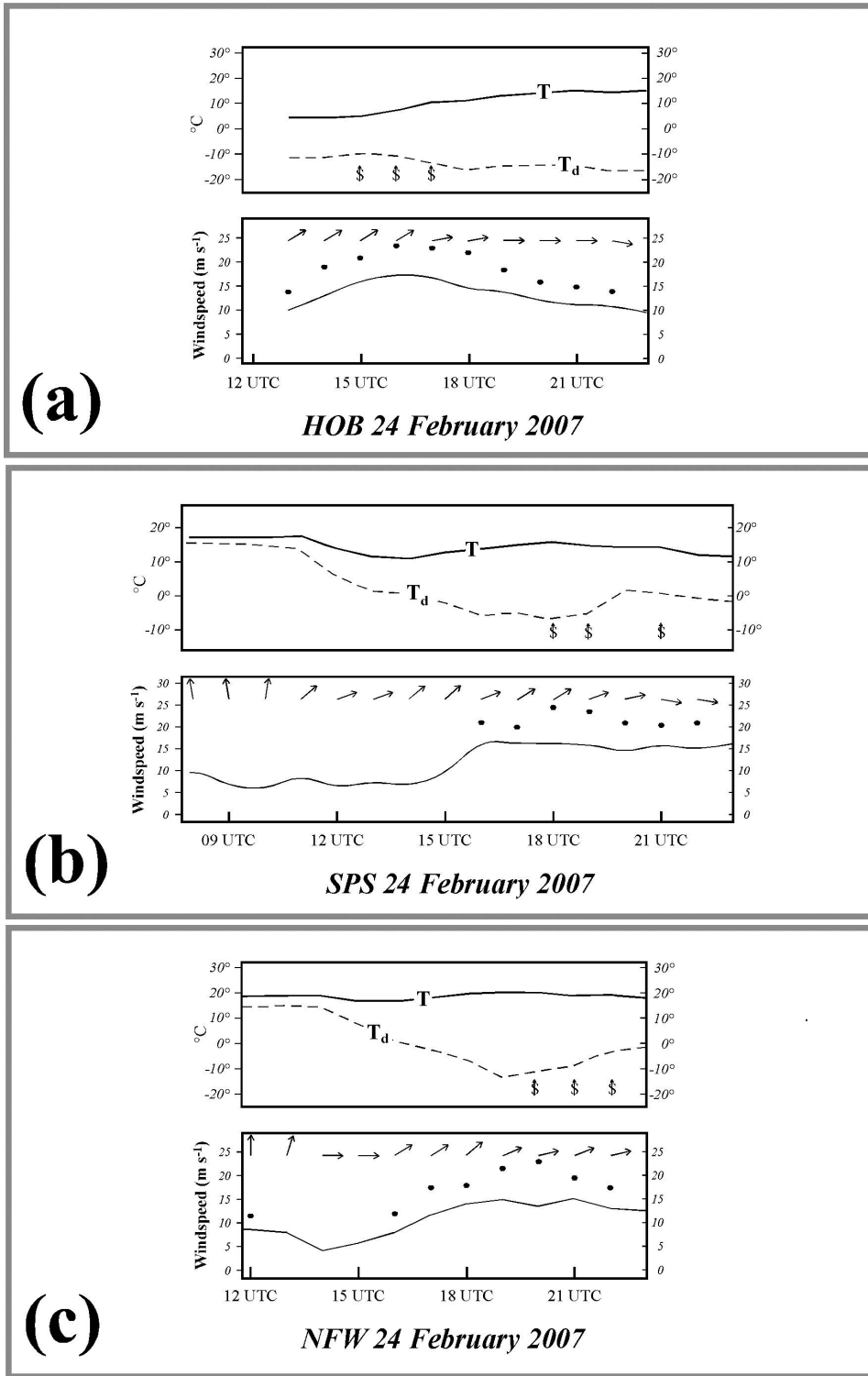


Fig. 5. (a) Meteorogram from Hobbs, New Mexico (HOB) from 1300 to 2200 UTC 24 February 2007. Top panel includes traces of temperature (solid line, scale on the side), dewpoint (dashed line, scale on the side), and sensible weather. Conventional symbol for dust is shown. Bottom panel shows wind direction (arrows), average wind speed (solid line with scale on sides), and peak gusts (black dots, with scale on sides). (b) Meteorogram for Wichita Falls, Texas (SPS) from 0800 – 2200 UTC 24 February 2007. Top and bottom panel as for Fig. 5a. (c) Meteorogram for Fort Worth, Texas (NFW) from 1200 – 2200 UTC 24 February 2007. Top and bottom panel as for Fig. 5a.

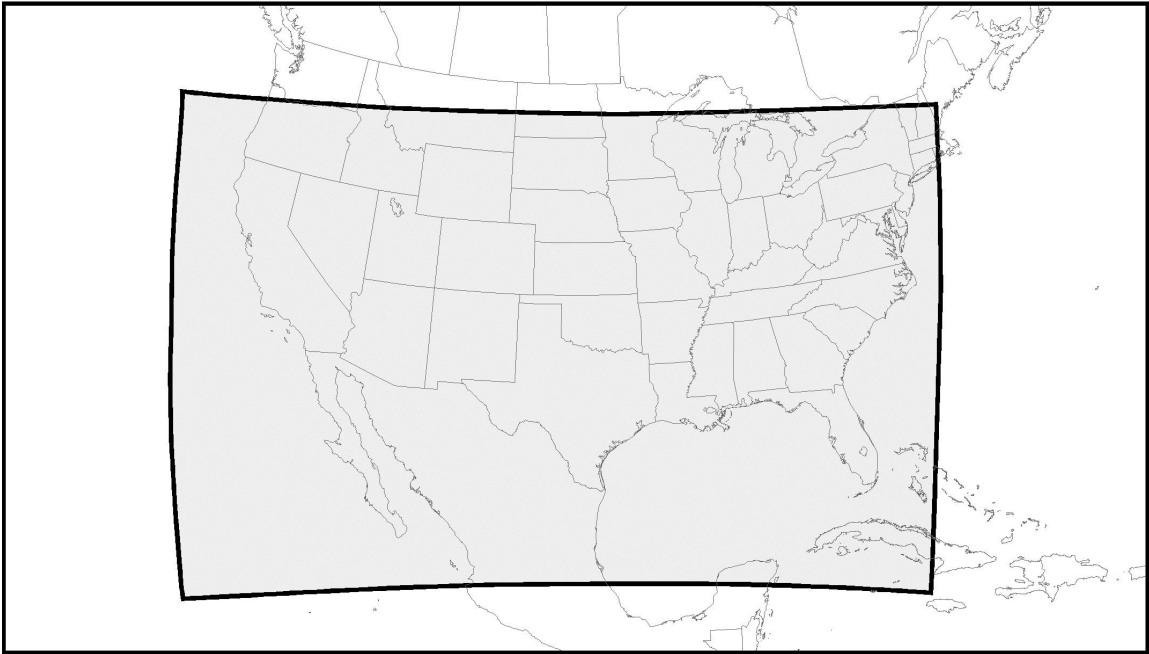


Fig. 6. Gray shaded area represents the domain for the WRF model run used in this study.

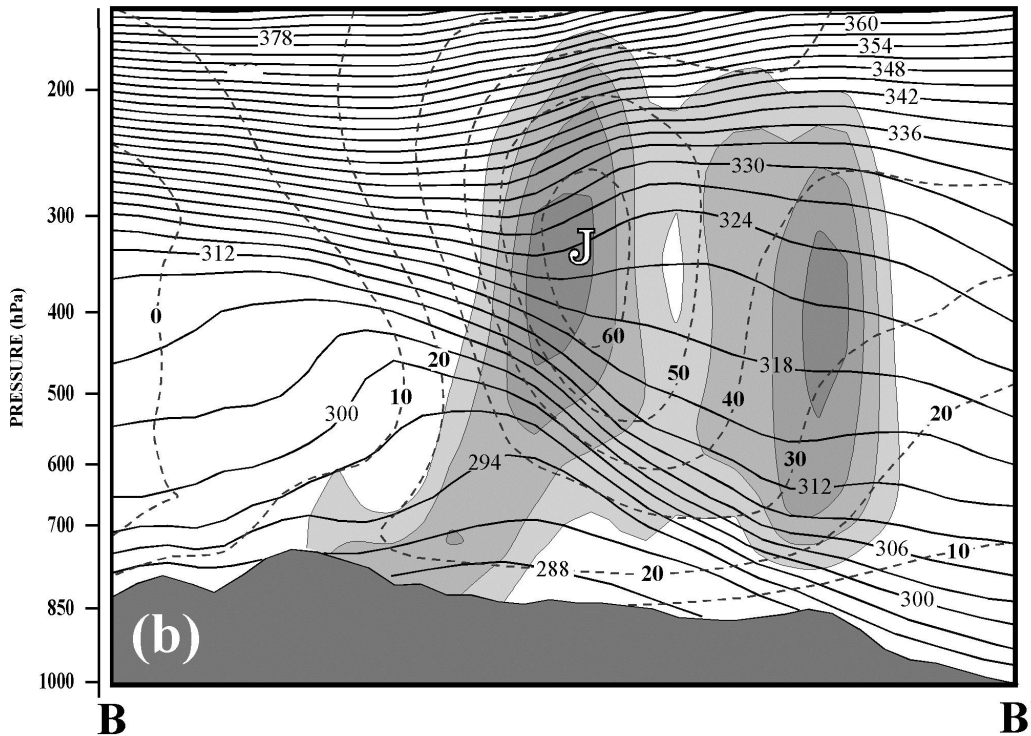
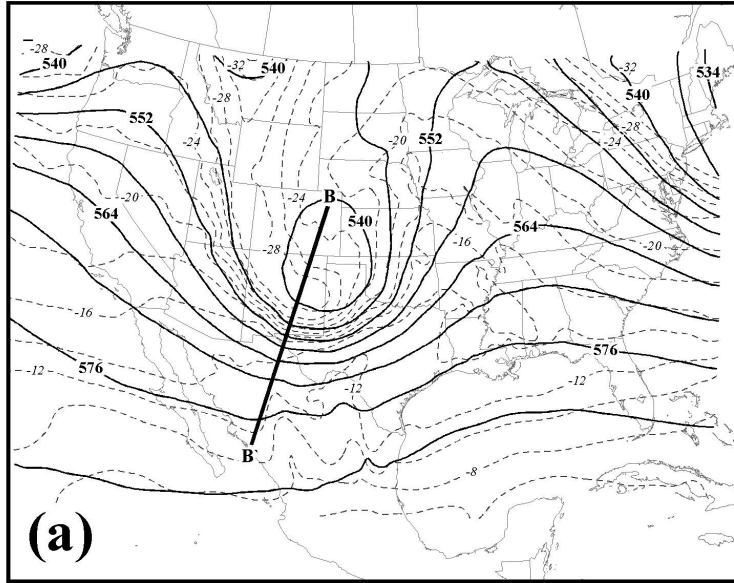


Fig. 7. (a) 12 h forecast of 500 hPa geopotential height (solid lines) and temperature (dashed lines) from the WRF model simulation valid at 1200 UTC 24 February 2007. Geopotential height and temperature labeled and contoured as in Fig. 2c. Vertical cross section along line B-B' is shown in Fig. 7b. (b) 12 h forecast vertical cross section along line B-B' in Fig. 7a from the WRF model simulation valid at 1200 UTC 24 February 2007. Solid lines are isentropes labeled and contoured as in Fig. 3. Dashed lines are isotherms normal to the cross section line labeled and contoured as in Fig. 3. Shading represents model forecast downward vertical motions at increments of  $5 \text{ cm s}^{-1}$  starting at  $-5 \text{ cm s}^{-1}$  decreasing to  $-20 \text{ cm s}^{-1}$ .

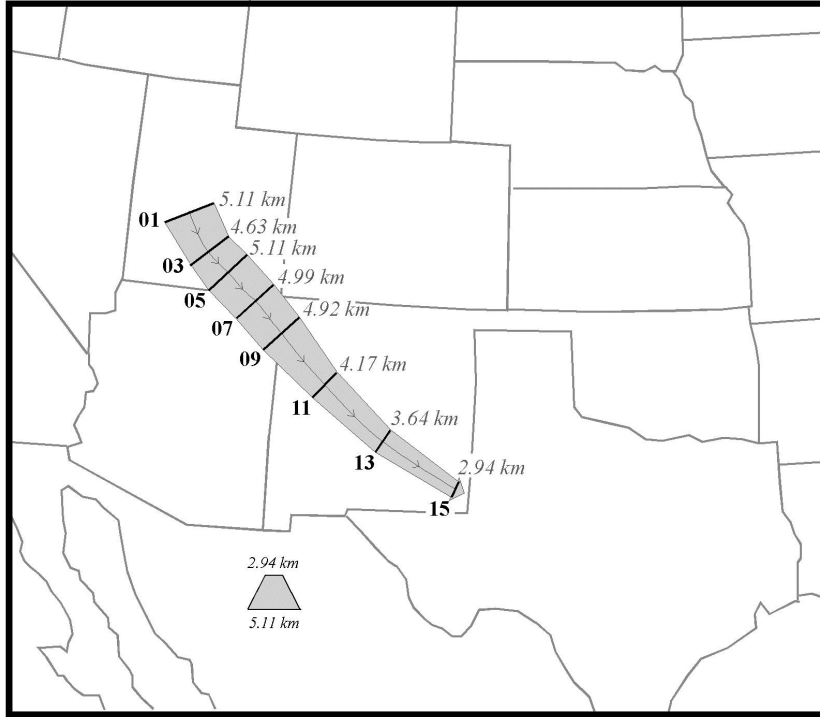


Fig. 8. Path of a representative trajectory, described in the text, from 0100 – 1500 UTC 24 February 2007. Thin line with arrow heads on it, in the middle of the shaded shaft, represents the geographic path of the trajectory. The width of the trajectory indicates the height of the air parcel at each two-hour time increment. Bold numbers to the left of the trajectory path indicate the UTC time at which the parcel is located at the intersection of the bold black lines and the trajectory path line. Italicized numbers to the right of the trajectory path indicate the elevation of the air parcel at each indicated time.

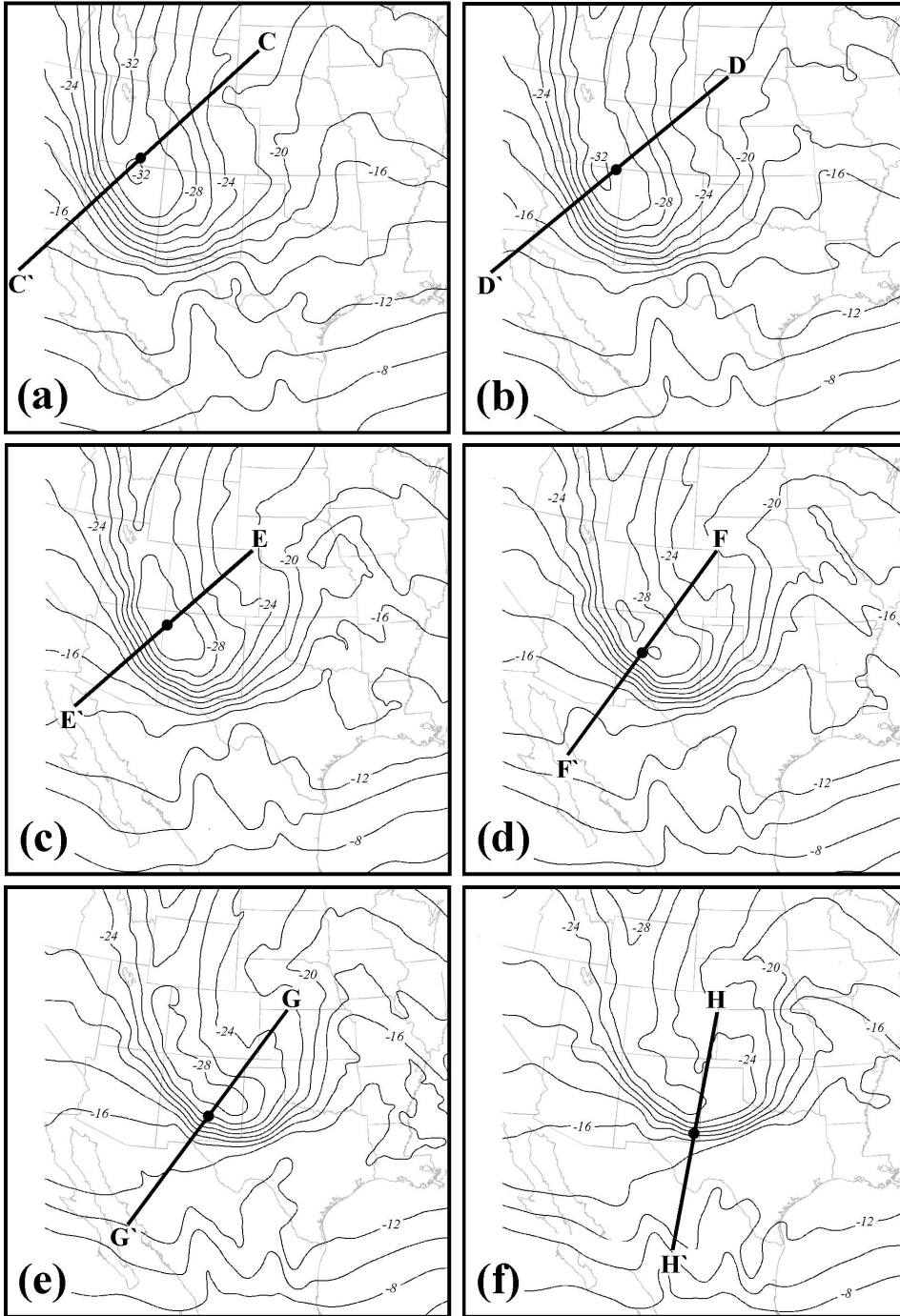


Fig. 9. (a) 5 h forecast of 500 hPa temperature from the WRF model valid at 0500 UTC 24 February 2007. The parcel whose trajectory path is shown in Fig. 8 is located at the black dot at this time. A vertical cross section along line C-C' is shown in Fig. 10a. (b) As for Fig. 9a but a 7 h forecast of 500 hPa temperature valid at 0700 UTC. The parcel whose trajectory path is shown in Fig. 8 is located at the black dot at this time. A vertical cross section along line D-D' is shown in Fig. 10b. (c) As for Fig. 9a but a 9 h forecast of 500 hPa temperature valid at 0900 UTC. The parcel whose trajectory path is shown in Fig. 8 is located at the black dot at this time. A vertical cross section along line E-E' is shown in Fig. 10c. (d) As for Fig. 9a but an 11 h forecast of 500 hPa temperature valid at 1100 UTC. The parcel whose trajectory path is shown in Fig. 8 is located at the black dot at this time. A vertical cross section along line F-F' is shown in Fig. 10d. (e) As for Fig. 9a but a 13 h forecast of 500 hPa temperature valid at 1300 UTC. The parcel whose trajectory path is shown in Fig. 8 is located at the black dot at this time. A vertical cross section along line G-G' is shown in Fig. 10e. (f) As for Fig. 9a but a 15 h forecast of 500 hPa temperature valid at 1500 UTC. The parcel whose trajectory path is shown in Fig. 8 is located at the black dot at this time. A vertical cross section along line H-H' is shown in Fig. 10f.

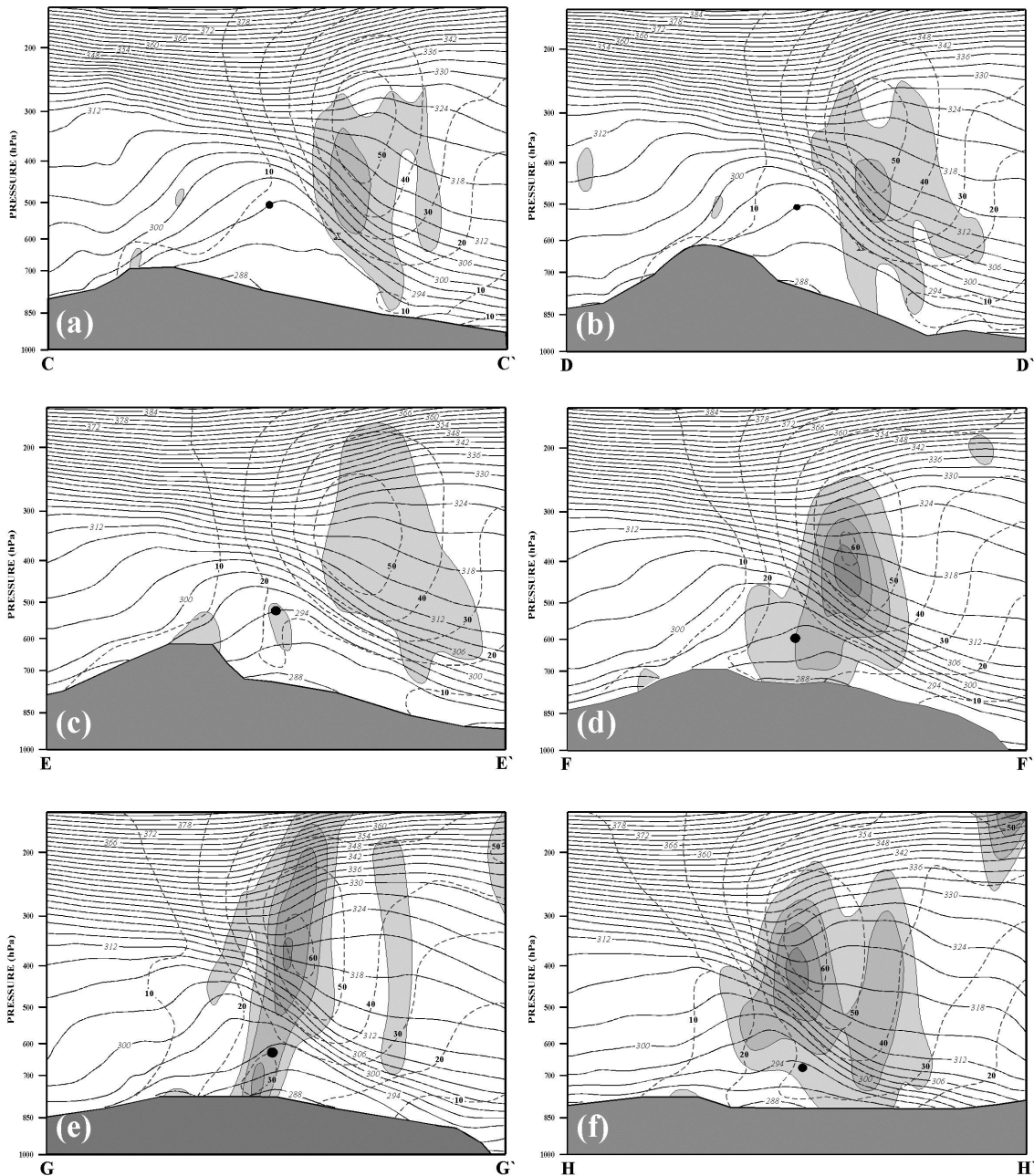


Fig. 10. (a) 5 h forecast vertical cross section of potential temperature (solid lines), isotachs normal to the cross section (dashed lines) and downward vertical velocity (shading) valid at 0500 UTC 24 February 2007 along line C-C' in Fig. 9a. Isentropes are labeled in K and contoured every 3 K. Isotachs are labeled in m s<sup>-1</sup> and contoured every 10 m s<sup>-1</sup> starting at 10 m s<sup>-1</sup>. Downward vertical motion labeled in cm s<sup>-1</sup> and shaded as in Fig. 7b. Black dot indicates the position of the representative air parcel at 0500 UTC. (b) As for Fig. 10a but for a 7 h forecast, along line D-D' in Fig. 9b, valid at 0700 UTC 24 February 2007. (c) As for Fig. 10a but for a 9 h forecast, along line E-E' in Fig. 9c, valid at 0900 UTC 24 February 2007. (d) As for Fig. 10a but for an 11 h forecast, along line F-F' in Fig. 9d, valid at 1100 UTC 24 February 2007. (e) As for Fig. 10a but for a 13 h forecast, along line G-G' in Fig. 9e, valid at 1300 UTC 24 February 2007. (f) As for Fig. 10a but for a 15 h forecast, along line H-H' in Fig. 9f, valid at 1500 UTC 24 February 2007.